考虑表面效应纳米压电双晶中波的频散分析*

黎 琪[1**] 胡 彪[1] 刘 娟[2]

([1] 贵州工程应用技术学院土木建筑工程学院,毕节,551700)([2] 西南交通大学力学与航空航天学院,成都,610031)

摘 要 基于非局部应变梯度理论探究了考虑表面弹性和表面残余应力的纳米压电双晶中波的频散特性,压电双晶的上下压电层暴露在电场之中并且整体沉积在粘弹性基底之上. 利用哈密顿原理和正弦剪切理论推导了控制方程,利用含非局部参数和长度尺度参数的尺度依赖本构关系得到了运动方程,带入谐波解求解相应的特征方程. 数值揭示了表面弹性和表面残余应力、尺度参数和波数以及粘弹性基底对压电双晶的作用规律. 研究表明,表面效应的存在对压电纳米双晶频率特性的研究至关重要,尺度参数和波数对频散特性具有耦合作用,弹性系数、阻尼系数和压电层厚度对频率的作用表现出区域性.

关键词 纳米压电双晶,频散特性,非局部应变梯度理论,表面效应,粘弹性基底

DOI:10.19636/j.cnki.cjsm42-1250/o3.2023.034

0 引言

砷化镓(GaAs)作为一种半导体材料被广泛的应用于军事、太空、光电子器件、日常通讯以及集成电路领域当中[1]. 砷化镓由于禁带宽、电子迁移率高和抗辐射等优点被用来制成太阳能电池,应用于航天飞机和纳米卫星组件中;又因为其具有速度快、高频性能和低功耗等特点广泛应用于微波通信以及光电集成领域;由于迁移率和高饱和电子速率的显著优势,砷化镓是制造射频功率放大器的主流衬底材料之一[2]. 随着射频器件往微型化和集成化方向发展,尺度效应对微纳米砷化镓衬底和结构动态特性的研究也亟需开展.

基于非经典连续介质力学理论,诸多学者关注了微纳米结构静动态力学特性的研究. 非局部理论和应变梯度理论被用来分析纳米结构的静动态行为[3,4]. Lim 等[5]发展了非局部应变梯度理论来解决非局部理论只能预测软化行为而应变梯度理论只能预测硬化行为的局限性问题. 与非局部理论和应变梯度理论相比,非局部应变梯度理论可以得出与实验[6,7]和分子动力学模拟[8,9]更加接近的结果. 自此以后,研究者利用非局部应变梯度理论探究了压电纳米结构的力学行为. 基于非局部应变梯度理论,压电纳米结构的屈曲[10-12]、弯曲[13,14]和振动[15,16]特性得到了进一步的研究. 结果表明,尺度效应对于压电纳米结构的屈曲、弯曲以及振动特性的影响显著. 近年来,不少学者也利用非局部应变梯度理论研究了压电纳米结构中波的传播特性. Ma 等[16-18]研究了多物理场作用下压电纳米板以及磁电弹纳米壳中波的频散特性. Wang 等[19]研究了沉积在粘弹性基底上的多孔功能梯度压电纳米壳中波的传播特性. Li 等[20]探究了不同孔隙分布与功能梯度指数对压电纳米板中波频散行为的影响. Ebrahimi 等[21]分析了含表面效应压电纳米板中波的传播特性. 以上的研究表明,非局部效应和应变梯度效应对压电纳米结构的频散特性具有不可忽略的作用,尺度参数的作用将使得压电纳米结构的频散行为更加剧烈. 此外,Hu 等[22-23]系统分析了多物理场作用下考虑表面效应的压电三明治纳米板中波的频散特性. 结果进一步表明,对压电纳米板频散特性的研究需要考虑表面效应的作用.

* 四川省自然科学基金项目(2022NSFSC2003)资助.
2023-07-24 收到修改稿, 2023-08-01 网络首发.

** 通讯作者. E-mail:1101620001@qq.com.

然而,以上的研究很少考虑表面残余应力和表面弹性的耦合作用,也鲜有关注压电层厚度和基底对频率作用的区域特性.

综上所述,基于非局部应变梯度理论揭示含表面效应压电纳米板的波动机理很有必要. 利用非局部应变梯度理论探究尺度效应、表面弹性以及表面残余应力、粘弹性基底等因素对纳米压电双晶中波动行为的影响机制. 基于正弦剪切变形理论和变分原理得到了压电双晶的控制方程,利用非局部应变梯度理论推导了尺度依赖的运动方程并带入谐波解求得相应的特征方程,数值揭示了表面效应、尺度效应以及粘弹性基底对纳米压电双晶频散特性的影响规律.

1 纳米压电双晶尺度依赖模型

1.1 物理模型

考虑表面效应纳米压电双晶的模型如图 1 所示. 压电双晶的上下表层是 GaAs 压电材料,中间层是 Mo 金属. Mo 金属的厚度 h_c 为 10 nm,GaAs 表面层的厚度 h_p 是 5 nm,压电双晶的长度 a 和宽度 b 均等于 200 nm. 压电双晶上下表层暴露在电场之中,并且沉积在粘弹性的基底之上. 文中后续上标 c,p,(b),(S),ac 和 se 分别代表与中间复合层,压电层,双晶体部分,表面效应,上压电制动层和下感应层有关的系数. 上下压电层的电边界条件是电学短路,其电路连接方式为并联.

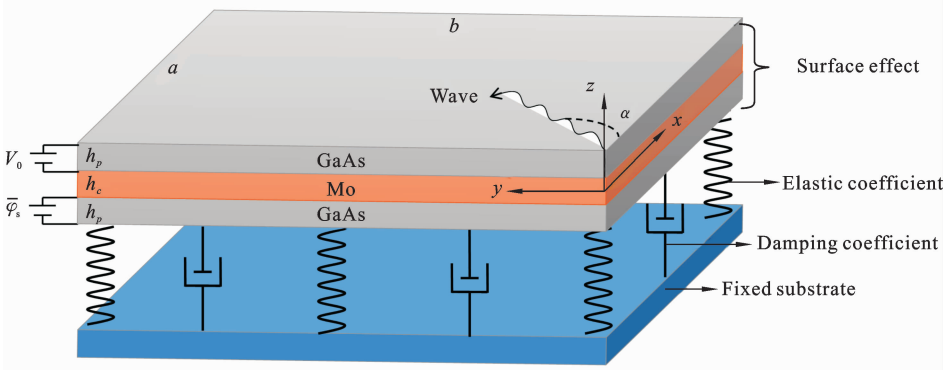

图 1 纳米压电双晶物理模型

Fig. 1 A physical model of nanoscale piezoelectric double crystal

1.2 理论建模

中间金属层的本构方程表示为[22]:

$$\begin{Bmatrix}\sigma^c_{xx}\\ \sigma^c_{yy}\\ \sigma^c_{xz}\\ \sigma^c_{yz}\\ \sigma^c_{xy}\end{Bmatrix}=\begin{bmatrix}p_{11} & p_{12} & 0 & 0 & 0\\ p_{12} & p_{22} & 0 & 0 & 0\\ 0 & 0 & p_{55} & 0 & 0\\ 0 & 0 & 0 & p_{44} & 0\\ & & & & p_{66}\end{bmatrix}\begin{Bmatrix}\varepsilon_{xx}\\ \varepsilon_{yy}\\ \gamma_{xz}\\ \gamma_{yz}\\ \gamma_{xy}\end{Bmatrix} \tag{1}$$

式中上标"c"代表了中间金属层的应力,压电层的本构方程表示为[23]:

$$\begin{Bmatrix}\sigma^p_{xx}\\ \sigma^p_{yy}\\ \sigma^p_{xz}\\ \sigma^p_{yz}\\ \sigma^p_{xy}\end{Bmatrix}=\begin{bmatrix}\bar{C}_{11} & \bar{C}_{12} & 0 & 0 & 0\\ \bar{C}_{12} & \bar{C}_{22} & 0 & 0 & 0\\ 0 & 0 & \bar{C}_{55} & 0 & 0\\ 0 & 0 & 0 & \bar{C}_{44} & 0\\ & & & & \bar{C}_{66}\end{bmatrix}\begin{Bmatrix}\varepsilon_{xx}\\ \varepsilon_{yy}\\ \gamma_{xz}\\ \gamma_{yz}\\ \gamma_{xy}\end{Bmatrix}-\begin{bmatrix}0 & 0 & \bar{e}_{31}\\ 0 & 0 & \bar{e}_{32}\\ \bar{e}_{15} & 0 & 0\\ 0 & \bar{e}_{24} & 0\\ 0 & 0 & 0\end{bmatrix}\begin{Bmatrix}E_x\\ E_y\\ E_z\end{Bmatrix} \tag{2}$$

式中上标"p"代表了压电层的应力.

$$\begin{Bmatrix}D_x\\ D_y\\ D_z\end{Bmatrix}=\begin{bmatrix}0 & 0 & \bar{e}_{15} & 0 & 0\\ 0 & 0 & 0 & \bar{e}_{24} & 0\\ \bar{e}_{31} & \bar{e}_{32} & 0 & 0 & 0\end{bmatrix}\begin{Bmatrix}\varepsilon_{xx}\\ \varepsilon_{yy}\\ \gamma_{xz}\\ \gamma_{yz}\\ \gamma_{xy}\end{Bmatrix}+\begin{bmatrix}\bar{s}_{11} & 0 & 0\\ 0 & \bar{s}_{22} & 0\\ 0 & 0 & \bar{s}_{33}\end{bmatrix}\begin{Bmatrix}E_x\\ E_y\\ E_z\end{Bmatrix} \tag{3}$$

考虑表面效应的压电本构方程为[22]：

$$\begin{Bmatrix}\sigma_{xx}^{(S)}\\ \sigma_{yy}^{(S)}\\ \sigma_{xz}^{(S)}\\ \sigma_{yz}^{(S)}\\ \sigma_{xy}^{(S)}\end{Bmatrix}=\begin{bmatrix}\bar{C}_{11}^{(S)} & \bar{C}_{12}^{(S)} & 0 & 0 & 0\\ \bar{C}_{12}^{(S)} & \bar{C}_{22}^{(S)} & 0 & 0 & 0\\ 0 & 0 & 0 & 0 & 0\\ 0 & 0 & 0 & 0 & 0\\ 0 & 0 & 0 & 0 & \bar{C}_{66}^{(S)}\end{bmatrix}\begin{Bmatrix}\varepsilon_{xx}\\ \varepsilon_{yy}\\ \gamma_{xz}\\ \gamma_{yz}\\ \gamma_{xy}\end{Bmatrix}-\begin{bmatrix}0 & 0 & \bar{e}_{31}^{(S)}\\ 0 & 0 & \bar{e}_{32}^{(S)}\\ \bar{e}_{15}^{(S)} & 0 & 0\\ 0 & \bar{e}_{24}^{(S)} & 0\\ 0 & 0 & 0\end{bmatrix}\begin{Bmatrix}E_x\\ E_y\\ E_z\end{Bmatrix}+\begin{Bmatrix}0\\ 0\\ \sigma^{(S)}\dfrac{\partial\hat{w}}{\partial x}\\ \sigma^{(S)}\dfrac{\partial\hat{w}}{\partial x}\\ 0\end{Bmatrix} \tag{4}$$

$$\begin{Bmatrix}D_x^{(S)}\\ D_y^{(S)}\\ D_z^{(S)}\end{Bmatrix}=\begin{bmatrix}0 & 0 & \bar{e}_{15}^{(S)} & 0 & 0\\ 0 & 0 & 0 & \bar{e}_{24}^{(S)} & 0\\ \bar{e}_{31}^{(S)} & \bar{e}_{32}^{(S)} & 0 & 0 & 0\end{bmatrix}\begin{Bmatrix}\varepsilon_{xx}\\ \varepsilon_{yy}\\ \gamma_{xz}\\ \gamma_{yz}\\ \gamma_{xy}\end{Bmatrix}+\begin{bmatrix}\bar{s}_{11}^{(S)} & 0 & 0\\ 0 & \bar{s}_{22}^{(S)} & 0\\ 0 & 0 & \bar{s}_{33}^{(S)}\end{bmatrix}\begin{Bmatrix}E_x\\ E_y\\ E_z\end{Bmatrix} \tag{5}$$

式中上标“(S)”表示与表面效应有关的参数，三明治纳米板的电势分布在文献[22]中给出，根据正弦剪切变形理论，得到位移场如下[23]：

$$\begin{cases}\bar{u}(x,y,z,t)=u(x,y,t)-z\dfrac{\partial w_b}{\partial x}-f(z)\dfrac{\partial w_s}{\partial x}\\ \bar{v}(x,y,z,t)=v(x,y,t)-z\dfrac{\partial w_b}{\partial y}-f(z)\dfrac{\partial w_s}{\partial y}\\ \bar{w}(x,y,z,t)=w_b(x,y,t)+w_s(x,y,t)\end{cases} \tag{6}$$

式中 u、v 代表 x 和 y 方向上中平面的位移，w_b 和 w_s 代表横向位移的弯曲分量和剪切分量，$f(z)=\dfrac{h}{\pi}\cdot\sin\left(\pi\cdot\dfrac{z}{h}\right)$ 代表形函数.

考虑电压和粘弹性基底的作用，阻尼造成的耗散包含在外力做功部分，这些载荷做功可定义为[23]：

$$\delta W=\int_0^a\int_0^b\left\{k_w(w_b+w_s)+c_d\left(\frac{\partial w_b}{\partial t}+\frac{\partial w_s}{\partial t}\right)+N_x^{\mathrm{E}}\frac{\partial^2(w_b+w_s)}{\partial x^2}+N_y^{\mathrm{E}}\frac{\partial^2(w_b+w_s)}{\partial y^2}\right\}(\delta w_b+\delta w_s)\mathrm{d}y\mathrm{d}x \tag{7}$$

式中 k_w，c_d 和 N_x^{E}、N_y^{E} 分别代表弹性系数，阻尼系数和 x、y 方向的电压作用.

结合金属层和压电层的本构方程与高阶剪切变形位移场，由变分原理得到应变能的变分 δU. 同样依据变分原理和高阶剪切位移场理论得到动能的变分 δV. 最终根据哈密顿原理 $\int_0^t\delta(U-V+W)\mathrm{d}t=0$，得到控制方程如下：

$$\frac{\partial(N_{xx}+N_{xx}^{(S)})}{\partial x}+\frac{\partial(N_{xy}+N_{xy}^{(S)})}{\partial y}=I_0\frac{\partial^2u}{\partial t^2\partial x}-J_1\frac{\partial^3w_s}{\partial t^2\partial x} \tag{8}$$

$$\frac{\partial(N_{xy}+N_{xy}^{(S)})}{\partial x}+\frac{\partial(N_{yy}+N_{yy}^{(S)})}{\partial y}=I_0\frac{\partial^2v}{\partial t^2}-I_1\frac{\partial^3w_b}{\partial t^2\partial y}-J_1\frac{\partial^3w_s}{\partial t^2\partial y} \tag{9}$$

$$\frac{\partial^2(M_{xx}^b+M_{xx}^{b(S)})}{\partial x^2}+2\frac{\partial^2(M_{xy}^b+M_{xy}^{b(S)})}{\partial x\partial y}+\frac{\partial^2(M_{yy}^b+M_{yy}^{b(S)})}{\partial y^2}-k_w(w_b+w_s)-c_d\left(\frac{\partial w_b}{\partial t}+\frac{\partial w_s}{\partial t}\right)-N_x^{\mathrm{E}}\nabla^2(w_b+w_s)=I_0\left(\frac{\partial^2w_b}{\partial t^2}+\frac{\partial^2w_s}{\partial t^2}\right)+I_1\left(\frac{\partial^3u}{\partial t^2\partial x}+\frac{\partial^3v}{\partial t^2\partial y}\right)-I_2\nabla\frac{\partial^2w_b}{\partial t^2}-J_2\nabla\frac{\partial^2w_s}{\partial t^2} \tag{10}$$

$$\frac{\partial^2(M_{xx}^s+M_{xx}^{s(S)})}{\partial x^2}+2\frac{\partial^2(M_{xy}^s+M_{xy}^{s(S)})}{\partial x\partial y}+\frac{\partial^2(M_{yy}^s+M_{yy}^{s(S)})}{\partial y^2}+\frac{\partial(Q_{xz}+Q_{xz}^{(S)})}{\partial x}+\frac{\partial(Q_{yz}+Q_{yz}^{(S)})}{\partial y}-k_w(w_b+w_s)-c_d\left(\frac{\partial w_b}{\partial t}+\frac{\partial w_s}{\partial t}\right)-N_x^{\mathrm{E}}\nabla^2(w_b+w_s)=I_0\left(\frac{\partial^2w_b}{\partial t^2}+\frac{\partial^2w_s}{\partial t^2}\right)+J_1\left(\frac{\partial^3u}{\partial t^2\partial x}+\frac{\partial^3v}{\partial t^2\partial y}\right)-J_2\nabla\frac{\partial^2w_b}{\partial t^2}-J_3\nabla\frac{\partial^2w_s}{\partial t^2} \tag{11}$$

$$\int_{-h_c/2-h_p}^{-h_c/2}\left(\frac{\partial D_x}{\partial x}\sin\left[\beta\left(-z-\frac{h_c}{2}\right)\right]+\frac{\partial D_y}{\partial y}\sin\left[\beta\left(-z-\frac{h_c}{2}\right)\right]+D_z\beta\cos\left[\beta\left(-z-\frac{h_c}{2}\right)\right]\right)\mathrm{d}z=0 \tag{12}$$

$$\int_{h_c/2}^{h_c/2+h_p}\left(\frac{\partial D_x}{\partial x}\sin\left[\beta\left(z-\frac{h_c}{2}\right)\right]+\frac{\partial D_y}{\partial y}\sin\left[\beta\left(z-\frac{h_c}{2}\right)\right]-D_z\beta\cos\left[\beta\left(z-\frac{h_c}{2}\right)\right]\right)\mathrm{d}z=0 \tag{13}$$

上述公式中，$N_{ij}^{(S)}$ 和 $M_{ij}^{b(S)}$、$M_{ij}^{s(S)}$、$Q_{ij}^{(S)}$ 分别表示由表面效应引起的力和力矩，M_{ij}^b 和 M_{ij}^s 代表由横向位移弯曲分量有关的力矩和剪切分量有关的力矩.

基于非局部应变梯度理论，并令有 $e_1=e_0=e$，压电本构方程可表示如下[5]：

$$\begin{cases}(1-\mu\nabla^2)\sigma_{ij}=(1-\eta\nabla^2)(c_{ijkl}\varepsilon_{kl}-e_{mij}E_m-\beta_{ij}\Delta T)\\(1-\mu\nabla^2)D_i=(1-\eta\nabla^2)(e_{ikl}\varepsilon_{kl}+s_{im}E_m-p_i\Delta T)\end{cases} \tag{14}$$

其中 $\mu=(ea)^2$ 代表非局部参数；$\eta=l^2$ 代表长度尺度参数，并令 $\Lambda=1-\mu\nabla^2$，$\Xi=1-\eta\nabla^2$. 金属层的尺度依赖本构方程在方程(14)中去掉电场部分即可得到，根据以上的尺度依赖本构方程在压电双晶截面上积分求得相应的力和力矩方程，带入控制方程(8)-(13)中得到运动方程如下：

$$\begin{aligned}&\Xi\Big\{(\hat{A}_{11}+A_{11}^{(S)})\frac{\partial^2 u}{\partial x^2}+(\hat{A}_{66}+A_{66}^{(S)})\frac{\partial^2 u}{\partial y^2}+[(\hat{A}_{12}+\hat{A}_{66})+(A_{12}^{(S)}+A_{66}^{(S)})]+\frac{\partial^2 v}{\partial x\partial y}-(\hat{B}_{11}+B_{11}^{(S)})\frac{\partial^3 w_b}{\partial x^3}\\&-[(\hat{B}_{12}+2\hat{B}_{66})+(B_{12}^{(S)}+2B_{66}^{(S)})]\frac{\partial^3 w_b}{\partial x\partial y^2}-(\hat{R}_{11}+R_{11}^{(S)})\frac{\partial^3 w_s}{\partial x^3}-[(\hat{R}_{12}+2\hat{R}_{66})+(R_{12}^{(S)}+2R_{66}^{(S)})]\\&\frac{\partial^3 w_s}{\partial x\partial y^2}\Big\}=\Lambda\Big(I_0\frac{\partial^2 u}{\partial t^2}-I_1\frac{\partial^3 w_b}{\partial t^2\partial x}-J_1\frac{\partial^2 w_s}{\partial t^2\partial x}\Big)\end{aligned} \tag{15}$$

$$\begin{aligned}&\Xi\Big\{[(\hat{A}_{12}+A_{66})+(A_{12}^{(S)}+A_{66}^{(S)})]\frac{\partial^2 u}{\partial x\partial y}+(\hat{A}_{66}+A_{66}^{(S)})\frac{\partial^2 v}{\partial x^2}+(\hat{A}_{22}+A_{66}^{(S)})\frac{\partial^2 v}{\partial y^2}-(\hat{B}_{22}+B_{22}^{(S)})\frac{\partial^3 w_b}{\partial y^3}-\\&[(\hat{B}_{12}+2\hat{B}_{66})+(B_{12}^{(S)}+2B_{66}^{(S)})]\frac{\partial^3 w_b}{\partial x^2\partial y}-(\hat{R}_{22}+R_{22}^{(S)})\frac{\partial^3 w_s}{\partial y^3}-[(\hat{R}_{12}+2\hat{R}_{66})+(R_{12}^{(S)}+2R_{66}^{(S)})]\\&\frac{\partial^3 w_s}{\partial x^2\partial y}\Big\}=\Lambda\Big(I_0\frac{\partial^2 v}{\partial t^2}-I_1\frac{\partial^3 w_b}{\partial t^2\partial y}-J_1\frac{\partial^3 w_s}{\partial t^2\partial y}\Big)\end{aligned} \tag{16}$$

$$\begin{aligned}&\Xi\Big\{(\hat{B}_{11}+B_{11}^{(s)})\frac{\partial^3 u}{\partial x^3}+[(\hat{B}_{12}+2\hat{B}_{66})+(B_{12}^{(S)}+2B_{66}^{(S)}]\frac{\partial^3 u}{\partial x\partial y^2}+(\hat{B}_{22}+B_{22}^{(S)})\frac{\partial^3 v}{\partial y^3}+[(\hat{B}_{12}+2\hat{B}_{66})+(B_{12}^{(S)}\\&+2B_{66}^{(S)})]\frac{\partial^3 v}{\partial x^2\partial y}-(\hat{D}_{11}+D_{11}^{(S)})\frac{\partial^4 w_b}{\partial x^4}-2[(\hat{D}_{12}+2\hat{D}_{66})+(D_{12}^{(S)}+2D_{66}^{(S)})]\frac{\partial^4 w_b}{\partial x^2\partial y^2}-(\hat{D}_{22}+D_{22}^{(S)})\\&\frac{\partial^4 w_s}{\partial y^4}-(\hat{G}_{11}+G_{11}^{(S)})\frac{\partial^4 w_s}{\partial x^4}-2[(\hat{G}_{12}+2\hat{G}_{66})+(G_{12}^{(S)}+2G_{66}^{(S)})]\frac{\partial^4 w_s}{\partial x^2\partial y^2}-(\hat{G}_{22}+G_{22}^{(S)})\frac{\partial^4 w_s}{\partial y^4}+(\hat{E}_{31}^{se(b)}+\\&\hat{E}_{31}^{se(S)})\nabla^2\bar{\varphi}_{se}+(\hat{E}_{31}^{ac(b)}+\hat{E}_{31}^{ac(S)})\nabla^2\bar{\varphi}_{ac}\Big\}+\\&\Lambda\Big\{-k_w(w_b+w_s)-c_d\Big(\frac{\partial w_b}{\partial t}+\frac{\partial w_s}{\partial t}\Big)-N_x^{\mathrm{E}}\nabla^2(w_b+w_s)\Big\}=\Lambda\Big[I_0\Big(\frac{\partial^2 w_b}{\partial t^2}+\frac{\partial^2 w_s}{\partial t^2}\Big)+\\&I_1\Big(\frac{\partial^3 u}{\partial t^2\partial x}+\frac{\partial^3 v}{\partial t^2\partial y}\Big)-I_2\nabla^2\frac{\partial^2 w_b}{\partial t^2}-J_2\nabla^2\frac{\partial^2 w_s}{\partial t^2}\Big]\end{aligned} \tag{17}$$

$$\begin{aligned}&\Xi\Big\{(\hat{R}_{11}+R_{11}^{(S)})\frac{\partial^3 u}{\partial x^3}+[(\hat{R}_{12}+2\hat{R}_{66})+(R_{12}^{(S)}+2R_{66}^{(S)}]\frac{\partial^3 u}{\partial x\partial y^2}+(\hat{R}_{22}+R_{22}^{(S)})\frac{\partial^3 v}{\partial y^3}+[(\hat{R}_{12}+2\hat{R}_{66})+(R_{12}^{(S)}\\&+2R_{66}^{(S)})]\frac{\partial^3 v}{\partial x^2\partial y}-(\hat{G}_{11}+G_{11}^{(S)})\frac{\partial^4 w_b}{\partial x^4}-2[(\hat{G}_{12}+2\hat{G}_{66})+(G_{12}^{(S)}+2G_{66}^{(S)})]\frac{\partial^4 w_b}{\partial x^2\partial y^2}-(\hat{G}_{22}+G_{22}^{(S)})\\&\frac{\partial^4 w_s}{\partial y^4}+g_\sigma^{(S)}\nabla^2 w_b-(\hat{H}_{11}+H_{11}^{(S)})\frac{\partial^4 w_s}{\partial x^4}-2[(\hat{H}_{12}+2\hat{H}_{66})+(H_{12}^{(S)}+2H_{66}^{(S)})]\frac{\partial^4 w_s}{\partial x^2\partial y^2}-(\hat{H}_{22}+H_{22}^{(S)})\\&\frac{\partial^4 w_s}{\partial y^4}+g_\sigma^{(S)}\nabla\nabla^2 w_s+\hat{T}_{55}\frac{\partial^2 w_s}{\partial x^2}+\hat{T}_{44}\frac{\partial^2 w_s}{\partial y^2}+[(\hat{E}_{32}^{se(b)}+\hat{E}_{15}^{se(S)})+\hat{E}_{32}^{se(S)}]\nabla^2\bar{\varphi}_{se}+[(\hat{E}_{32}^{ac(b)}+\hat{E}_{15}^{ac})+\hat{E}_{32}^{ac(S)}]\\&\nabla^2\bar{\varphi}_{ac}\Big\}+\Lambda\Big\{-k_w(w_b+w_s)-c_d\Big(\frac{\partial w_b}{\partial t}+\frac{\partial w_s}{\partial t}\Big)-N_x^{\mathrm{E}}\nabla^2(w_b+w_s)\Big\}=\Lambda\Big[I_0\Big(\frac{\partial^2 w_b}{\partial t^2}+\frac{\partial^2 w_s}{\partial t^2}\Big)+\\&J_1\Big(\frac{\partial^3 u}{\partial t^2\partial x}+\frac{\partial^3 v}{\partial t^2\partial y}\Big)-J_2\nabla^2\frac{\partial^2 w_b}{\partial t^2}-J_3\nabla^2\frac{\partial^2 w_s}{\partial t^2}\Big]\end{aligned} \tag{18}$$

$$\Xi\Big(\hat{H}_{31}^{se}\frac{\partial^2 w_b}{\partial x^2}+\hat{H}_{32}^{se}\frac{\partial^2 w_b}{\partial y^2}+(\hat{K}_{31}^{se}+\hat{F}_{15}^{se})\frac{\partial^2 w_s}{\partial x^2}+(\hat{K}_{32}^{se}+\hat{F}_{24}^{se})\frac{\partial^2 w_s}{\partial y^2}+\hat{F}_{11}^{se}\frac{\partial^2\bar{\varphi}_{se}}{\partial x^2}+\hat{F}_{22}^{se}\frac{\partial^2\bar{\varphi}_{se}}{\partial y^2}+\hat{F}_{33}^{se}\bar{\varphi}_{se}\Big)=0 \tag{19}$$

$$\Xi\Big(\hat{H}_{31}^{ac}\frac{\partial^2 w_b}{\partial x^2}+\hat{H}_{32}^{ac}\frac{\partial^2 w_b}{\partial y^2}+(\hat{K}_{31}^{ac}+\hat{F}_{15}^{ac})\frac{\partial^2 w_s}{\partial x^2}+(\hat{K}_{32}^{ac}+\hat{F}_{24}^{ac})\frac{\partial^2 w_s}{\partial y^2}+\hat{F}_{11}^{ac}\frac{\partial^2\bar{\varphi}_{ac}}{\partial x^2}+\hat{F}_{22}^{ac}\frac{\partial^2\bar{\varphi}_{ac}}{\partial y^2}+\hat{F}_{33}^{ac}\bar{\varphi}_{ac}\Big)=0 \tag{20}$$

上述公式中上标“(S)”代表了与表面效应作用有关的参数. 由于研究的压电纳米双晶包含了上下压电层的作用，上压电层用作制动器，其相关参数用上标“ac”表示；下压电层用作感应器，其相关参数用上标

"*se*"表示. 假设谐波具有指数位移场

$$\begin{cases}\{u,v,w_b,w_s,\bar{\varphi}_{se},\bar{\varphi}_{ac}\}^{\mathrm{T}}=h_0\,\mathrm{e}^{\mathrm{i}(k_1x+k_2y-\omega t)}\\ h_0=\{u_0,v_0,w_{b0},w_{s0},\bar{\varphi}_{se0},\bar{\varphi}_{ac0}\}^{\mathrm{T}}\end{cases}\tag{21}$$

式中 h_0 代表波动幅值.

把方程(21)代入方程(15)～(20),得到特征方程为:

$$([K]+\omega[C]-\omega^2[M])\{h_0\}=\{0\}\tag{22}$$

非零解存在的条件是:

$$|[K]+\omega[C]-\omega^2[M]|=0\tag{23}$$

求解上述方程即可得到纳米压电双晶的频散关系.

2　数值结果及分析

压电材料为 GaAs,它的材料参数在表 1 中给出[24]. GaAs 的表面弹性参数由下面的表达式给出:$c_{ij}^{(\mathrm{S})}=\dfrac{c_{ij}}{2}\cdot p_1\cdot 10^{-9}$,其中 p_1 代表表面弹性系数,上下压电层的表面残余应力为 $\sigma^{(\mathrm{S})}$,表面残余应力的范围一般小于 10 N/m. 中间金属层 Mo 的弹性模量为 329 GPa,密度为 10280 kg/m^3,泊松比为 0.34.

表 1　压电材料 GaAs 的材料参数[24]

Table 1　Material parameters of piezoelectric material GaAs

	GaAs
Elastic constants c_{ij} (GPa)	$c_{11}=119$, $c_{22}=119$, $c_{12}=53.8$, $c_{13}=53.8$, $c_{33}=119$, $c_{44}=59.5$, $c_{55}=59.5$, $c_{66}=59.5$
Piezoelectric coefficients e_{ij} (C/m^2)	$e_{31}=e_{32}=0$, $e_{33}=0$, $e_{14}=e_{25}=-0.16$
Static dielectric constants s_{ij} (10^{-8} F/m)	$s_{11}=11$, $s_{33}=11$
Mass density ρ_p (kg/m^3)	$\rho_p=5310$

2.1　有效性验证

纳米级压电双晶的验证工作在已有的文献中还比较少见,而关于压电纳米板的实验研究也在文献中鲜有见到,Ma 等[18]基于非局部理论分析压电纳米板频散特性的研究与纳米压电双晶密切相关. 研究纳米压电双晶时,把中间金属层以及上下的压电层替换为 $BiTiO_3$-$CoFe_2O_4$,忽略长度尺度参数的作用后得到压电双晶的频散曲线如图 2 所示. 由图可知,本文的研究结果与 Ma 等的研究结果较为一致,证明了本文基于非局部应变梯度理论探究纳米压电双晶频散特性的研究是可行而有效的.

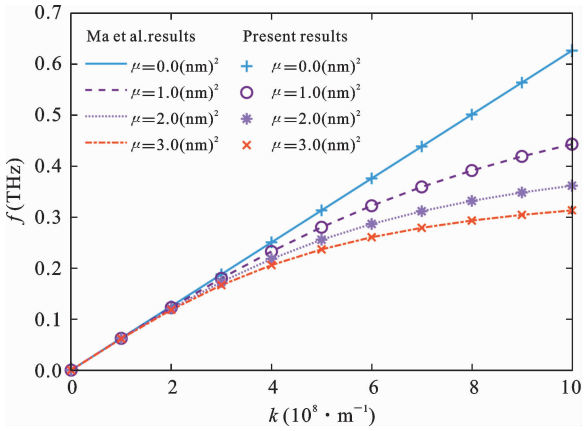

图 2　纳米级压电双晶的模型验证

Fig. 2　Model validation of nanoscale piezoelectric bimorphs

2.2　数值讨论

图 3 中给出了表面弹性系数和表面残余应力对压电双晶中波传播频率的影响. 由图可知,随着表面残余应力的增大压电双晶的频率逐渐增大,因为增大正的表面残余应力在一定程度上提高了压电双晶的刚度. 此外,当表面残余应力固定,压电双晶的频率随着表面弹性系数的增大而增大,其原因是表面弹性系数的存在增大了整个压电层的弹性模量. 由此可见,对于纳米压电双晶,考虑表面效应对其频率的影响是必不可少的. 值得注意的是,当表面残余应力较小时($k=6\times10^8$ m^{-1},$h_p=5$ nm),表面弹性系数对频率的影响比较轻微,该结果为降低表面弹性

系数对纳米压电双晶的影响提供了另一条思路. 图中频率曲线斜率的突变,不是由于表面残余应力的临界值造成,而与波数和压电层厚度的共同作用有关.

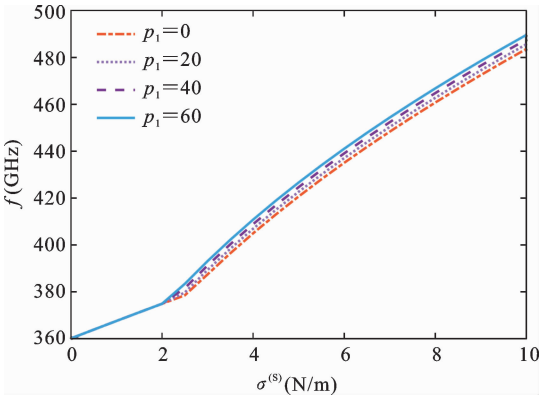

图 3 表面弹性系数和表面残余应力对频率的影响

Fig. 3 The influence of surface elasticity coefficient and surface residual stress on frequency

图 4 中给出了非局部理论和应变梯度理论框架下尺度参数对频率比的作用,频率比是指考虑非局部效应时的频率 ω_N 和不考虑非局部效应时的频率 ω_L 的比值. 图 4(a)中的结果表明,当非局部参数不为 0 nm^2 时,无论波数的在哪一个范围,压电双晶的频率比都小于 1,验证了非局部参数的软化效应. 当波数固定时,频率比会随着非局部参数的增大而逐渐降低,而且非局部参数越大,频率比降低得会越剧烈. 此外,非局部参数对频率比的影响还和波数有密切的联系. 当波数较小($k=1\times10^8$ m^{-1})时,非局部参数对频率比的影响较小;当波数较大($k=7\times10^8$ m^{-1})时,随着非局部参数的增大,压电双晶的频率比接近 0.6,这说明波数较大时,非局部参数的软化效应更加明显. 图 4(b)中的结果显示,无论波数的取值多少,长度尺度参数的存在都会使得压电双晶的频率比大于 1,这是因为长度尺度参数的硬化作用. 结果还表明,随着长度尺度参数的增大,频率比有所增加,然而,频率比的这种增加还和波数有密切联系. 当波数较小($k=1\times10^8$ m^{-1})时,随长度尺度参数的增加,频率比略微增加;当波数较小时,长度尺度参数的硬化效应比较微弱. 由此可知,当 $k<1\times10^8$ m^{-1} 且长度尺度参数较小时,尺寸效应对频率的影响几乎可以忽略;当波数较大($k=7\times10^8$ m^{-1})时,压电双晶的频率比会随着长度尺度参数的增加而显著增加,其增幅达到 0.6 倍. 这说明,大波数情况下,长度尺度参数的硬化效应具有不可忽略的意义.

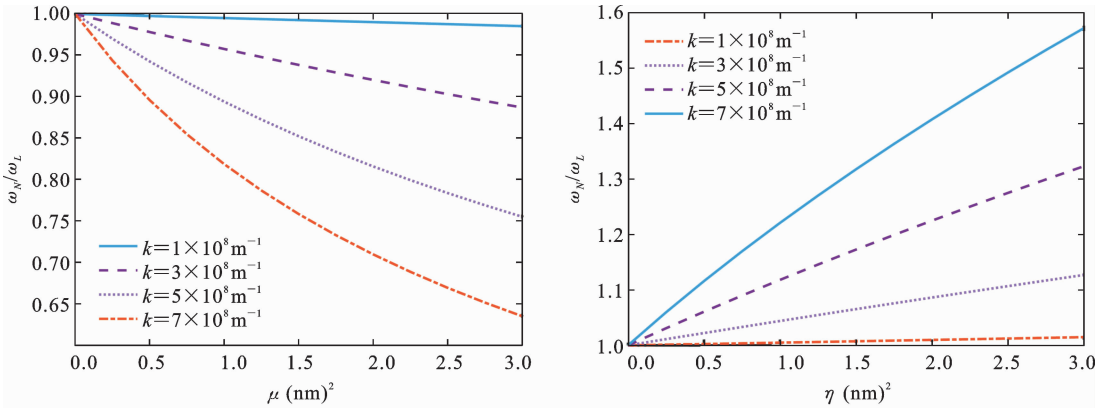

(a) 非局部理论 (b) 应变梯度理论

(a) Nonlocal theory (b) Strain gradient theory

图 4 非局部理论和应变梯度理论框架下尺度参数对频率比的影响

Fig. 4 The influence of scale parameters on frequency ratio under the nonlocal theoretical and strain gradient theory framework

图 5(a)中的结果表明,随着非局部参数的增大,波频率降低;随着长度尺度参数的增大,波频率增大. 当非局部参数为 0 nm^2 时,长度尺度参数对频率的增幅最大;同理,当长度尺度参数为 0 nm^2 时,

非局部参数对频率的降幅最大. 此外，波频率在非局部参数较小时降幅较大，而随着非局部参数的增大，它对压电双晶的软化效应逐渐变弱. 同时，长度尺度参数的硬化作用也受到非局部参数的影响. 由此可见，非局部参数和长度尺度参数对频率具有耦合作用. 图 5(b)中的结果显示，当非局部参数固定，波的频率随着长度尺度参数的增大而增大；当长度尺度参数不变，波的频率随着非局部参数的增大而降低. 结果表明，当长度尺度参数不变且 $\Delta\mu=1\ \mathrm{nm}^2$ 时，非局部参数对频率的降幅逐渐减小，说明非局部参数的软化作用逐渐减弱. 当 μ 从 0 nm^2 变化到 1 nm^2，非局部参数的软化效应最为显著，说明当长度尺度参数不变，非局部参数较小时其带来的软化效应较明显. 当非局部参数为 0 nm^2 时，频率在长度尺度参数的作用下得到了最大的增强，而当非局部参数为 3 nm^2 时，长度尺度参数对频率的提升较小；也就是说当非局部参数存在时，长度尺度参数对频率的增强作用会受到影响.

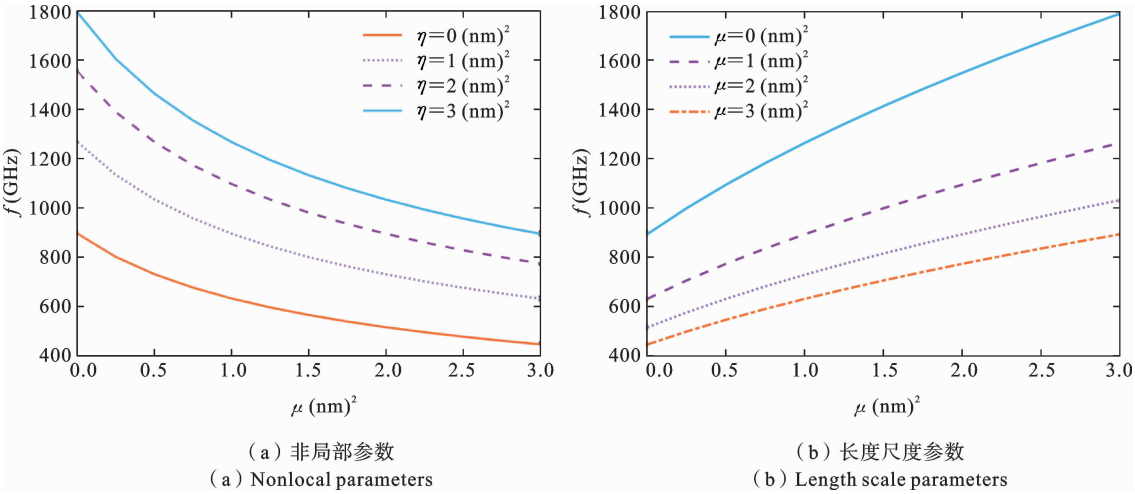

（a）非局部参数　（b）长度尺度参数
（a）Nonlocal parameters　（b）Length scale parameters

图 5　非局部应变梯度理论框架下非局部参数和长度尺度参数对频率的耦合作用

Fig. 5　The coupling effect of nonlocal parameters and length scale parameters on frequency under the framework of nonlocal strain gradient theory

弹性系数、阻尼系数和压电层厚度对频率的影响在图 6 中给出. 图中的结果表明，随着压电层厚度的增大，纳米压电双晶的频率显著降低，这意味着压电双晶在制备时需要重点关注厚度的准确度以及均

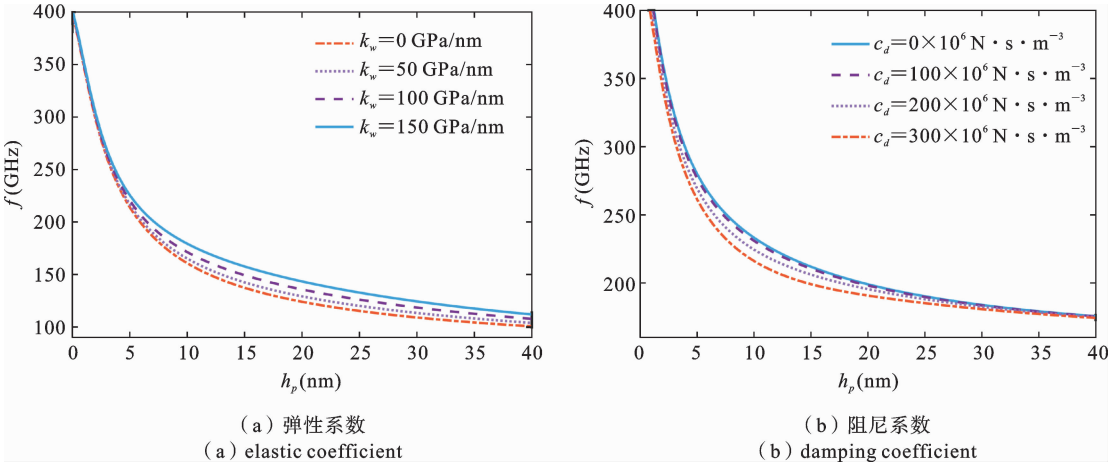

（a）弹性系数　（b）阻尼系数
（a）elastic coefficient　（b）damping coefficient

图 6　弹性系数、阻尼系数和压电层厚度对频率的影响

Fig. 6　The influence of elastic coefficient, damping coefficient, and piezoelectric layer thickness on frequency

匀性. 图 6(a)的结果表明,压电双晶的频率随着粘弹性基底中弹性系数的增大而增大,因为增大弹性系数提高了压电双晶的刚度. 研究中以粘弹性基底模拟压电双晶和固定基板之间的粘接作用,也就是说选用刚度更大的粘接剂对频率的影响更大. 需要注意的是,弹性系数对频率的增强作用在压电层厚度较小时不明显,该作用表现出一定的区域特性. 图 6(b)的结果显示,增大粘弹性基底的阻尼系数,将导致压电双晶的频率降低,因为增大阻尼对波在结构中的传播起到了阻滞作用. 需要关注的是,阻尼系数的这种作用在压电层厚度较大或者较小时都表现得不明显,其与弹性系数对频率的作用类似表现出了区域特性. 以上的结果表明,在纳米压电双晶的应用过程中应根据其厚度和目标频率的需要来选择符合要求的粘接剂.

3 结论

基于非局部应变梯度理论分析了含表面效应的纳米压电双晶中波的频散特性,重点讨论了表面弹性和表面残余应力、非局部参数和长度尺度参数以及弹性系数和阻尼系数对频率的作用,得到的主要结论如下:

(1) 表面弹性系数和表面残余应力的存在提高了压电双晶的频率,可以通过改善表面残余应力的方法来影响表面弹性系数对频率的作用.

(2) 非局部参数对频率的软化效应和长度尺度参数对频率的硬化效应都受到波数的限制,非局部参数和长度尺度参数对频率的作用存在竞争机制.

(3) 增大弹性系数能提高压电双晶的频率,而阻尼系数的增大降低了波的频率;受压电层厚度的影响,弹性系数和阻尼系数对频率的作用表现出区域特性.

参考文献

[1] 孔令奇. 砷化镓(GaAs)材料压痕响应的试验研究[D]. 吉林大学, 2019. (Kong L Q. Experimental research of indentation testing of GaAs material[D]. Ji-Lin University, 2019. (in Chinese))

[2] 陈玉梅, 杨耒. 初应力下压电半导体板中 SH 波的传播特性[J]. 固体力学学报, 2022, 43(04): 467-476. (Cen Y M, Yang L. SH wave propagation in piezoelectric semiconductor plate with initial stress[J]. Chinese Journal of Solid Mechanics, 2022, 43(04): 467-476. (in Chinese))

[3] 李明, 吕刘飞, 郑华升, 方康. 磁场对不同温度场中输流悬臂碳纳米管颤振稳定性的影响[J]. 固体力学学报, 2021, 42(01): 87-93. (Li M, Lv L F, Zheng H S, Fang K. Magnetic field effect on flutter stability of a fluid- conveying cantilevered carbon nanotube under different temperature fields[J]. Chinese Journal of Solid Mechanics, 2021, 42(01): 87-93. (in Chinese))

[4] 邹星, 张波, 张旭, 王宇星, 沈火明. 含尺度效应的功能梯度三明治微梁振动、弯曲与屈曲特性研究[J]. 固体力学学报, 2022, 43(03): 344-359. (Zou X, Zhan B, Zhan X, Wang Y X, Shen H M. Research on vibration, bending and buckling characteristics of functionally graded sandwich microbeams with size effects[J]. Chinese Journal of Solid Mechanics, 2022, 43(03): 344-359. (in Chinese))

[5] Lim C W, Zhang G, Reddy J N. A higher-order nonlocal elasticity and strain gradient theory and its applications in wave propagation[J]. Journal of the Mechanics and Physics of Solids, 2015, 78: 298-313.

[6] Karami B, Shahsavari D, Li L. Hygrothermal wave propagation in viscoelastic graphene under in-plane magnetic field based on nonlocal strain gradient theory[J]. Physica E: Low-dimensional Systems and Nanostructures, 2018, 97: 317-327.

[7] Karami B, Janghorban M, Tounsi A. Variational approach for wave dispersion in anisotropic doubly-curved nanoshells based on a new nonlocal strain gradient higher order shell theory[J]. Thin-Walled Structures, 2018, 129: 251-264.

[8] Habibi M, Mohammadgholiha M, Safarpour H. Wave propagation characteristics of the electrically GNP-reinforced nanocomposite cylindrical shell[J]. Journal of the Brazilian Society of Mechanical Sciences and Engineering, 2019, 41(5): 1-15.

[9] 戴光韬, 李皓男, 姚林泉. 纳米圆轴在弹性介质中的扭转振动分析[J]. 固体力学学报, 2021, 42(05):

599-611. (Dai G T, Li H N, Yao L Q. Torsional vibration analysis of round nanoshaft in elastic medium [J]. Chinese Journal of Solid Mechanics, 2021, 42 (05): 599-611. (in Chinese))

[10] Wang X H, Wang P Y, Jiang W, Wu F Q, Kiani M, Arefi M. Mathematical and computer simulation for Electro-Magneto-Thermo-Elastic buckling of the porous nano system[J]. Structural engineering and mechanics, 2021, 80(2): 231-242.

[11] Ebrahimi F, Barati M R. Magnetic field effects on buckling characteristics of smart flexoelectrically actuated piezoelectric nanobeams based on nonlocal and surface elasticity theories[J]. Microsystem Technologies, 2018, 24 (5): 2147-2157.

[12] Wang Y, Hong W W, Smitt J. Bending and vibration analysis of the FG circular nanoplates subjected to hygro-thermo-electrical loading based on nonlocal strain gradient theory[J]. International Journal of Structural Stability and Dynamics, 2023, 23(02): 2350017.

[13] Zhang L, Guo J H, Xing Y M. Bending analysis of functionally graded one-dimensional hexagonal piezoelectric quasicrystal multilayered simply supported nanoplates based on nonlocal strain gradient theory [J]. Acta Mechanica Solida Sinica, 2021, 34(2): 237-251.

[14] 罗秋阳，李成. 考虑非局部应变梯度效应的轴对称压电纳米圆板热-力-电耦合振动[J]. 振动工程学报，2022, 35(05): 1118-1129. (Luo Q Y, Li C. Thermo-mechanical electrical coupling vibration of axisymmetric piezoelectric nanocircular plate considering nonlocal strain gradient effect[J]. Journal of Vibration Engineering, 2022, 35(05): 1118-1129. (in Chinese))

[15] 罗天喜. 基于非局部应变梯度理论的压电纳米多层结构的力电耦合特性分析[D]. 南昌航空大学，2021. (Luo T X. Analysis of Electromechanical Coupling Characteristics of Piezoelectric Nano-Multilayer Structure Based on Nonlocal Strain Gradient Theory [D]. Nanchang Hangkong University, 2021. (in Chinese))

[16] Ma L H, Ke L L, Wang Y Z, Wang Y S. Wave propagation in magneto-electro-elastic nanobeams via two nonlocal beam models[J]. Physica E: Low-dimensional Systems and Nanostructures, 2017, 86: 253-261.

[17] Ma L H, Ke L L, Reddy J N, Yang J, Kitipornchai S, Wang Y S. Wave propagation characteristics in magneto-electro-elastic nanoshells using nonlocal strain gradient theory [J]. Composite Structures, 2018, 199: 10-23.

[18] Ma L H, Ke L L, Wang Y Z, Wang Y S. Wave propagation analysis of piezoelectric nanoplates based on the nonlocal theory[J]. International Journal of Structural Stability and Dynamics, 2018,18(4):1-19.

[19] Wang X T, Liu J, Hu B, Li Z N, Zhang B. Wave propagation in porous functionally graded piezoelectric nanoshells resting on a viscoelastic foundation [J]. Physica E: Low-dimensional Systems and Nanostructures, 2023,151: 115615.

[20] Li Z N, Liu J, Hu B, Wang Y X, Shen H M. Wave propagation analysis of porous functionally graded piezoelectric nanoplates with a visco-Pasternak foundation[J]. Applied Mathematics and Mechanics (English Edition), 2023, 44(01): 35-52.

[21] Ebrahimi F, Dabbagh A. Wave propagation analysis of embedded nanoplates based on a nonlocal strain gradient-based surface piezoelectricity theory[J]. The European Physical Journal Plus, 2017, 132(11): 449.

[22] Hu B, Liu J, Wang Y X, Zhang B, Shen H M. Wave propagation analysis of functionally graded graphene-reinforced piezoelectric sandwich nanoplates via nonlocal strain gradient theory [J]. International Journal of Structural Stability and Dynamics, 2022, 23(07): 2350070.

[23] Hu B, Liu J, Wang Y X, Zhang B, Wang J, Shen H M. Study on wave dispersion characteristics of piezoelectric sandwich nanoplates considering surface effects [J]. Applied Mathematics and Mechanics (English Edition), 2022, 43(09): 1339-1354.

[24] Pedro S, Garcia-Gancedo L, Ford C J B, Barnes C H W, Griffiths J P, Jones G A C, Flewitt A J. Guided propagation of surface acoustic waves and piezoelectric field enhancement in ZnO/GaAs systems [J]. Journal of Applied Physics, 2011, 110(10): 103501.

Dispersion Analysis of Waves in Nanoscale Piezoelectric Double Crystals Considering Surface Effects

Qi Li[1] Biao Hu[1] Juan Liu[2]

([1] *School of Civil Engineering, Guizhou University of Engineering Science, Bijie*, 551700)

([2] *School of Mechanics and Aerospace Engineering, Southwest Jiaotong University, Chengdu*, 611756)

Abstract Due to progress in micro and nano technologies, nanoscale piezoelectric bimorphs have gained extensive popularity in various fields such as nanosensors, nanoactuators, nanoscale energy recovery devices, and nanoresonators. With a decrease in size, the influence of scale effect becomes more prominent. The aim of this research was to investigate the scale effect on the frequency characteristics of nanoscale piezoelectric bimorphs according to scale-dependent theory. This work may broaden our understanding of the wave characteristics of piezoelectric nanostructures. On the basis of nonlocal strain gradient theory, the wave dispersion properties in nanoscale piezoelectric bimorphs were studied, taking into account surface elasticity and residual stress. The upper and lower piezoelectric layers of the bimorphs were subjected to an electric field and deposited on a viscoelastic substrate. The control equation was derived based on Hamilton's principle and sinusoidal shear theory. The equation of motion was derived according to the scale-dependent constitutive equation with nonlocal and length scale parameters, and the corresponding characteristic equation was solved by incorporating harmonic solutions. The obtained numerical results revealed the effects of surface elasticity, residual stress, scale parameters, wave number, and viscoelastic substrate on piezoelectric bimorphs. The research showed that the dispersion properties of piezoelectric bimorphs were influenced by a combination of surface residual stress and surface elastic coefficient. The existence of surface effects was found to be essential for the investigation of the frequency properties of piezoelectric bimorphs. Scale parameters and wave number also had a combined effect on dispersion characteristics, and the influences of elastic coefficient, damping coefficient, and piezoelectric layer thickness on frequency exhibited regional characteristics. Therefore, it is possible to use appropriate substrate materials to regulate the center frequency of piezoelectric bimorphs. This work contributes to the theoretical research on the dispersion mechanism of piezoelectric nanoresonators and provides useful reference for the design and manufacturing of piezoelectric nanofilters.

Key words nanoscale piezoelectric bimorphs, frequency dispersion characteristics, nonlocal strain gradient theory, surface effect, viscoelastic substrate